

UNIVERSITY of CALIFORNIA  
SANTA CRUZ

**THE DISCOVERY OF ECLIPSING BINARIES AMONG MAIN  
SEQUENCE STARS IN NGC 6752**

A thesis submitted in partial satisfaction of the  
requirements for the degree of

BACHELOR OF SCIENCE

in

ASTROPHYSICS

by

**Carlos A. Hernandez III**

10 June 2009

Copyright © by  
Carlos A. Hernandez III  
2009

## CONTENTS

List of Figures	3
List of Tables	4
Dedication	5
Acknowledgements	6
1. Introduction	7
2. Observations and Data Reduction	10
2.1. Observations At The Telescope	10
2.2. Reduction	15
3. Photometry Of Stars	17
3.1. Background	17
3.2. Selecting PSF Stars	17
3.3. PSF Fitting To Measure Stellar Brightness: Daophot	20
3.4. Matching Stars Measured On Different Frames: Daomatch	21
3.5. Combining Photometry For Stars Measured On Different Frames: Daomaster	23
4. Discussion	23
4.1. E/I vs. Chi	23
4.2. Star Inspection	24
4.3. Periodic Signals	25
5. Color-Magnitude Diagram	26
5.1. Background	26
5.2. Candidates on the CMD	26
5.3. Artificial Star	27
5.4. Detections	29
6. Conclusion	31
References	32

## LIST OF FIGURES

1	Flat-Field Schematic	17
2	PSF	18
3	FWHM	19
4	Subtracted Image	22
5	E/I vs. Chi	24
6	Candidate Stars	25
7	Short CMD of NGC 6752	27
8	Deep CMD of NGC 6752	28
9	Artificial Star	28
10	Star 5996 Light Curve	29
11	Star 5000730 Light Curve	30
12	Star 5996 and 5000730 Location	30

## LIST OF TABLES

1	NGC 6752 Observations	10
2	NGC 6752 Observations (Continued)	11
3	NGC 6752 Observations (Continued)	12
4	NGC 6752 Observations (Continued)	13
5	NGC 6752 Observations (Continued)	14
6	NGC 6752 Observations (Continued)	15
7	Light Curve Parameters	30

*To my family,  
who have always been there for me*

#### ACKNOWLEDGEMENTS

I want to thank Dr. Enrico Ramirez-Ruiz for involving me in this research project including his suggestions along the way. Dr. Jason Kalirai for all the technical help during the first months of this project and graduate student Kate Ruben for the data reduction. In addition, I want to thank Kyle Kaplan for practical suggestions and discussions about basic astronomy concepts that were relevant to this research. Lastly, I truly want to thank Dr. Michael Bolte for his generous help in all aspects of the project. His time and honorable advice were highly valued making this an interesting and engaging research right from the start.

# THE DISCOVERY OF ECLIPSING BINARIES AMONG MAIN SEQUENCE STARS IN NGC 6752

CARLOS A. HERNANDEZ III

ABSTRACT. We have conducted CCD photometry from NGC 6752 with the use of the 0.9 and 4 meter telescopes at the Cerro Tololo Inter-American Observatory (CTIO). A total 199 images in the I and V-band were obtained in the years of 1993 and 1994. With past findings of binaries by other groups, we anticipate to be reinforcing a few of the same detections provided that we have well gain data coverage with better time-series analysis. However, two binaries have been discovered concealing periods of  $P = 0.61988$  and  $P = 0.24209$  days that give an amplitude of  $M_0 = 0.32120$  and  $M_0 = 1.48840$  respectively. Their binary classification type is still undetermined but further descriptions will be presented in a near future publication. Additionally, we represent in this paper a recent deep color-magnitude diagram of this cluster.

## 1. INTRODUCTION

To date, object NGC 6752 is one of about 158 globular star clusters that are bound by the Milky Way Galaxy<sup>1</sup>. Commonly located in the halo of galaxies, a globular cluster (GC) is a gravitationally bound system that can vary in the number of stars that comprises one. Such a number can range from several thousands to millions in a single cluster. In contrast with stars found in open clusters, stars from GCs tend to be very old in age with low metallicity. Metallicity measures the abundance of elements heavier than helium in the star's atmosphere, and do to their ages and lack of metals, stars in these colossal systems are classified as Population II stars<sup>2</sup>. In fact, based on age comparison, they are inclined to be one of the oldest objects in the universe. Consequently though up to the mid 90's, there

---

<sup>1</sup>This number was given in 2007 in <http://seds.org/spider/spider/mwgc/mwgc.html>

<sup>2</sup>Population I and II are distinct by their metallicity and age (M. H. Jones & R. J. A. Lambourne 2003)



was a great discrepancy on age determinations of GCs. Before the discovery of an accelerating universe, it was firmly believed that the universe held an age of about 8-9 Gyrs, while GCs concealed almost twice that. Most were confident that GCs perhaps attained the miscalculation because calculating for their ages was a very complex process. And so, one of the project's motivation was achieving a revised age of GCs by studying the reminiscence of dying stars called white dwarfs that belong to the cluster group. These hold as fossil records that one can trace back and therefore determine the age of a star cluster. Unfortunately, because white dwarfs are relatively faint, they were very difficult to find and the concept was abandoned. Soon after followed the discovery of an accelerating universe that caused its age to be revised, and hence need not worry about previous age determinations of GCs.

Nevertheless, the study of GCs carried additional interest that brought further ambition with conjunction to the project. Taking a different direction, it was believed that because GCs are in a compact state, it seemed reasonable to suspect that a black hole could evolve in their inner cores. In this general situation, a black hole would consume near present stars and consequently cause a cataclysmic collapse of the cluster. However, after numerous observations black holes were never found, causing for an explanation of what sustains GCs from a critical catastrophe based on their appearance<sup>3</sup>.

It was then hypothesized that maybe binary stars in the cores could possibly be the key to an anti-collapse. Binaries are two orbiting stars that are trapped by their mutual gravitational attraction and are likely expected in crowded regions like in GCs. With presumed binaries in the center, stars around the vicinity would interact with them and eventually sling shot back out with greater kinetic energies than what they commenced with at first. As binaries settle deeper into the cores having accrued more potential energy from promiscuous interactions, stars ejected back into the medium could even exceed the escape velocity of the cluster. This occurrence of increasing the stars velocity dispersion in and around the cluster

---

<sup>3</sup>The presence of black holes in globular clusters is still a hot debate.

would cause it to expand in size, and overtime cool off and contract. This balance mechanism for equilibrium would repeat, neglecting the act of collapse. For that reason, the purpose of the project was to find binaries in the heart of NGC 6752, specifically eclipsing binaries (EB). EB's are two orbiting stars that block each others starlight as they orbit one another from our line of sight here on Earth. These stars can be found via their light curves by graphing the stars magnitude as a function of time. Therefore, finding dips in these plots give the argument that EB's are present.

The discovery of NGC 6752 was made by the Scottish astronomer James Dunlop in the early 19th century, and first cataloged as Dunlop 295 <sup>4</sup>. Out of the several bound clusters, this one was chosen for many practical reasons. For one, it is one of the closest to our sun with a distance of only 4 kpc (Harris 1996). As part of the Pavo constellation it is positioned 27° below the southern horizon with an RA of 19h 10m 51s and DEC of -59° 58' 55". This makes it a convenience for long visibility do to its location in the southern hemisphere. With an approximate age of  $13.8 \pm 1.1$  Gyrs (Gratton et al. 2003), it carries  $[F_e/H] = -1.43 \pm 0.04$  in metallicity (Gratton et al. 2003) making it one of the oldest and poor in abundance. Finally, it carries a low foreground reddening of  $E(B - V) = 0.04$  (Harris 1996) making it ideal for data taking. Reddening deals with the dust obscuration that lies in between us and the observed object. The lower this number, the better.

With earlier work done by a few members of the CASE group, eleven variables were detected from NGC 6752 (Thompson et al. 1999). But recently, 17 variables were identified with three previously detected, and 14 newly discovered (Kaluzny & Thompson). In their findings, several binary eclipses were cataloged along with multiple SX Phoenicis, blue horizontal branch (BHB), and extreme horizontal branch stars (EHB). SX Phoenicis are sub-dwarf stars smaller than the size of our sun that pulsate with some periodicity. BHB are blue giant stars that have used all of their hydrogen supply and have begun their helium burning process. EHB hold

<sup>4</sup>This is provided in <http://seds.org/spider/spider/mwgc/n6752.html>

the same characteristics but are the most extreme type of stars in the horizontal branch, passed the main sequence phase in the Hertzsprung-Russell diagram. In future publication, we are expected to find these similar detections hopefully with newly discovered binaries. Therefore, the objective of this research was to find a considerable amount of EBs to study their properties, and learn more about their inner environments that make such GC systems sustain their form as seen today. Results will be provided early this year.

## 2. OBSERVATIONS AND DATA REDUCTION

**2.1. Observations At The Telescope.** Images from this cluster were taken with two telescopes in the years of June '93 and July '94. Located in Chile at 22,000 feet in altitude, the 0.9m telescope was the smallest of the two, and has a pixel scale of  $0''.396 \text{ pixel}^{-1}$  with a field size of  $6'.8 \times 6'.8 \text{ arcmin}^5$ . The 4m Blanco telescope contains  $0''.478 \text{ pixel}^{-1}$  obtaining  $16'.3 \times 16'.3 \text{ arcmin}$  for a field of view. The exposure on the images spanned from 3 to 900 seconds for reasons of having a broad range in time. A total of 93 V-band and 106 I-band images were attain and acknowledged for data analysis. The raw images were conventionally formatted as a Flexible Image Transport System–FITS as the standard file extension. Table (1) below is a list of all images taken on the years of '93 and '94. The table consists of 199 images in the I and V-band combined.

TABLE 1. NGC 6752 Observations

JD (2449000.0)	RA	DEC	EXP (sec)	FWHM
153.7695949	19:08:22.00	-60:03:50.00	100	2.7
153.7771528	19:08:22.00	-60:03:50.00	900	3.0
153.7891782	19:08:21.00	-60:03:58.00	900	2.9
153.8012037	19:08:21.00	-60:04:05.00	900	3.0
153.8133218	19:08:21.00	-60:04:11.00	900	2.9
153.8253356	19:08:21.00	-60:04:17.00	900	3.0
153.8373611	19:08:22.00	-60:04:18.00	900	2.8
153.8502778	19:08:22.00	-60:04:12.00	900	2.8

<sup>5</sup>The field of view for the 0.9 meter has now changed to  $13'.5 \times 13'.5$ . For a table of the latest changes go to <http://www.ctio.noao.edu/telescopes/36/0-9m.html>

Table 2: NGC 6752 Observations (Continued)

JD (2449000.0)	RA	DEC	EXP (sec)	FWHM
153.8623032	19:08:22.00	-60:04:08.00	900	2.8
153.8743171	19:08:22.00	-60:04:03.00	900	2.7
152.8435185	19:08:12.00	-60:04:04.00	10	4.2
154.5853935	19:06:28.00	-60:03:54.00	10	2.9
154.5879629	19:06:28.00	-60:03:49.00	10	2.7
154.5896875	19:06:28.00	-60:03:45.00	10	2.8
154.7596181	19:08:26.00	-60:04:16.00	100	2.0
154.8674653	19:08:26.00	-60:04:23.00	900	2.5
154.8794792	19:08:26.00	-60:04:27.00	900	2.6
154.8914931	19:08:26.00	-60:04:31.00	900	2.7
154.9043287	19:08:26.00	-60:04:35.00	900	2.7
152.8867129	19:08:12.00	-60:04:05.00	300	3.5
152.8918634	19:08:12.00	-60:03:59.00	300	3.4
154.7671759	19:08:26.00	-60:04:16.00	900	2.3
154.7801968	19:08:26.00	-60:04:14.00	900	2.4
154.7921991	19:08:26.00	-60:04:12.00	900	2.1
154.8042014	19:08:26.00	-60:04:08.00	900	2.4
152.8978704	19:08:12.00	-60:03:53.00	300	3.5
152.9029745	19:08:12.00	-60:04:07.00	300	3.4
152.9080556	19:08:12.00	-60:04:12.00	300	3.5
153.7670486	19:08:22.00	-60:03:50.00	10	3.0
542.7489282	19:08:30.87	-60:04:06.60	900	3.5
542.7597697	19:08:30.99	-60:04:07.20	900	3.3
542.7706099	19:08:30.88	-60:04:07.40	900	3.4
542.7783704	19:08:31.41	-60:04:07.10	120	3.4
542.7850417	19:08:31.40	-60:04:07.30	900	4.1
542.8067153	19:08:31.33	-60:04:07.90	900	4.6
542.8244688	19:08:31.65	-60:04:06.40	10	4.2
542.8249931	19:08:31.55	-60:04:06.40	10	4.4
543.5810116	19:08:26.41	-60:04:14.70	10	4.2
541.8363125	19:08:24.76	-60:04:07.20	900	4.2
543.5925625	19:08:31.84	-60:04:02.20	900	3.4
543.6359409	19:08:31.16	-60:03:55.20	10	3.4
543.6437083	19:08:31.16	-60:03:54.20	900	3.5
543.6545486	19:08:30.90	-60:03:52.80	900	3.0
543.6611713	19:08:30.77	-60:03:50.30	120	3.0
543.7157882	19:08:30.86	-60:03:51.20	10	3.7
543.7176366	19:08:30.86	-60:03:51.20	120	4.1
543.7242558	19:08:30.88	-60:03:51.10	900	4.3
543.7350949	19:08:30.89	-60:03:52.10	900	4.1
543.7459306	19:08:30.82	-60:03:53.00	900	4.0
542.6184340	19:08:32.15	-60:04:05.30	10	3.0
543.7525046	19:08:30.96	-60:04:01.30	10	4.1
543.7539398	19:08:30.97	-60:04:01.30	120	4.2

Table 3: NGC 6752 Observations (Continued)

JD (2449000.0)	RA	DEC	EXP (sec)	FWHM
543.7604826	19:08:30.95	-60:04:00.90	900	4.5
543.7713276	19:08:30.79	-60:04:01.10	900	5.1
543.7821887	19:08:30.77	-60:04:00.70	900	4.1
544.6336701	19:12:55.55	-59:58:53.70	10	4.7
544.6402268	19:12:55.46	-59:58:52.10	120	4.5
544.6468044	19:12:55.43	-59:58:52.00	900	5.6
544.6576481	19:12:55.20	-59:58:50.70	900	4.8
544.6684792	19:12:55.01	-59:58:49.10	900	4.3
542.6211181	19:08:32.08	-60:04:05.20	120	3.4
544.6750602	19:11:59.38	-59:58:49.30	3	4.1
544.6771030	19:11:59.53	-59:58:50.00	15	4.2
544.6776887	19:11:59.46	-59:58:49.80	15	4.2
544.6782766	19:11:59.45	-59:58:49.70	15	4.3
544.6788681	19:11:59.48	-59:58:49.50	15	4.5
544.6794815	19:11:59.40	-59:58:50.00	15	4.9
544.7241042	19:08:32.02	-60:03:53.90	10	3.0
544.7260602	19:12:56.02	-59:58:49.50	120	3.9
544.7326887	19:12:56.03	-59:58:49.50	900	4.0
544.7435289	19:12:55.98	-59:58:49.10	900	3.7
542.6277743	19:08:32.08	-60:04:04.50	900	3.4
544.7543669	19:12:56.01	-59:58:49.10	900	3.6
544.7613355	19:12:55.73	-59:58:49.90	185.58	3.5
544.7683947	19:12:56.48	-59:58:50.20	900	3.3
544.7792338	19:12:56.19	-59:58:50.40	900	3.3
544.7900741	19:12:56.25	-59:58:51.80	900	3.3
544.8011574	19:12:56.11	-59:58:51.70	900	3.4
542.6386134	19:08:31.99	-60:04:03.10	900	3.6
542.6494537	19:08:31.80	-60:04:01.00	900	3.4
542.6616458	19:08:31.73	-60:03:55.30	900	3.1
542.6724826	19:08:31.34	-60:03:53.00	900	3.2
542.6833252	19:08:31.40	-60:03:51.80	900	4.0
154.7572454	19:08:27.00	-60:04:16.00	10	2.0
155.7554514	19:08:24.00	-60:03:58.00	200	4.0
155.7602199	19:08:24.00	-60:03:57.00	200	4.4
155.7639121	19:08:24.00	-60:03:57.00	200	4.2
155.8967939	19:08:24.00	-60:03:58.00	200	4.3
155.9004514	19:08:24.00	-60:03:58.00	200	4.4
155.9041088	19:08:24.00	-60:03:58.00	200	4.6
157.7125694	19:11:58.00	-59:59:31.00	600	3.8
158.7921296	19:11:59.00	-59:59:15.00	120	3.2
158.7978009	19:11:59.00	-59:59:15.00	600	3.6
152.9130093	19:08:12.00	-60:04:25.00	200	2.9
152.9169213	19:08:13.00	-60:04:31.00	200	2.7
152.9210069	19:08:13.00	-60:04:35.00	200	2.7

Table 4: NGC 6752 Observations (Continued)

JD (2449000.0)	RA	DEC	EXP (sec)	FWHM
152.9249074	19:08:13.00	-60:04:39.00	200	2.8
153.6444329	19:08:22.00	-60:03:59.00	6	2.5
153.6589005	19:08:22.00	-60:03:57.00	100	2.9
153.6655671	19:08:22.00	-60:03:58.00	600	2.9
153.6741435	19:08:22.00	-60:04:03.00	600	3.2
153.6827083	19:08:22.00	-60:04:08.00	600	3.4
153.6912732	19:08:22.00	-60:04:12.00	600	3.2
153.6998380	19:08:21.00	-60:04:16.00	600	3.2
153.8818519	19:08:22.00	-60:04:02.00	6	2.7
153.8870255	19:08:22.00	-60:04:02.00	100	2.9
153.8941319	19:08:22.00	-60:04:00.00	600	3.4
153.9026852	19:08:22.00	-60:03:54.00	600	3.2
153.9112037	19:08:22.00	-60:03:47.00	600	3.1
153.9182060	19:08:23.00	-60:03:46.00	300	2.7
153.9232755	19:08:23.00	-60:04:12.00	300	2.9
153.9283796	19:08:23.00	-60:04:07.00	300	3.0
152.8409954	19:08:12.00	-60:04:05.00	10	3.3
153.9334375	19:08:23.00	-60:04:01.00	300	3.1
154.5709259	19:06:28.00	-60:03:54.00	8	3.2
154.5738310	19:06:28.00	-60:03:49.00	8	2.6
154.5756481	19:06:28.00	-60:03:44.00	8	2.7
154.6995023	19:08:12.00	-60:04:06.00	600	2.5
154.7080440	19:08:12.00	-60:04:10.00	600	2.5
154.7231366	19:08:27.00	-60:04:08.00	600	2.3
154.7317593	19:08:27.00	-60:04:13.00	600	2.2
154.7403241	19:08:27.00	-60:04:16.00	600	2.4
152.8475116	19:08:12.00	-60:04:05.00	200	3.4
154.7459143	19:08:27.00	-60:04:15.00	60	1.9
154.7480208	19:08:27.00	-60:04:15.00	8	1.9
154.8329051	19:08:26.00	-60:04:10.00	600	2.6
154.8414352	19:08:26.00	-60:04:17.00	600	2.4
154.8499653	19:08:26.00	-60:04:23.00	600	2.4
152.8516435	19:08:12.00	-60:03:59.00	200	3.2
152.8559838	19:08:12.00	-60:03:54.00	200	3.2
152.8602546	19:08:12.00	-60:04:10.00	200	3.3
152.8645718	19:08:12.00	-60:04:15.00	200	4.1
152.8686111	19:08:12.00	-60:04:20.00	200	4.2
152.8725463	19:08:12.00	-60:04:25.00	200	4.1
542.7052280	19:08:31.11	-60:03:54.50	600	3.2
542.7125926	19:08:31.13	-60:03:54.80	600	3.3
542.7202743	19:08:30.88	-60:04:05.60	600	3.3
542.7276412	19:08:30.87	-60:04:05.20	600	3.2
542.7349988	19:08:30.92	-60:04:05.70	600	3.1
542.8314595	19:08:31.44	-60:04:05.90	10	3.4

Table 5: NGC 6752 Observations (Continued)

JD (2449000.0)	RA	DEC	EXP (sec)	FWHM
542.8319988	19:08:31.43	-60:04:05.90	10	3.9
542.8325278	19:08:31.44	-60:04:05.80	10	4.2
542.8340833	19:08:31.46	-60:04:05.70	120	4.4
542.8390255	19:08:31.53	-60:04:05.50	600	4.4
541.6386702	19:08:25.80	-60:04:09.50	262.82	2.7
542.8538252	19:08:31.93	-60:04:03.60	600	4.5
542.8614583	19:08:31.96	-60:04:02.90	600	4.5
543.6627766	19:08:30.72	-60:03:50.20	10	3.0
543.6642581	19:08:30.60	-60:03:50.30	3	3.1
543.6656331	19:08:30.54	-60:03:50.10	120	2.6
543.6705255	19:08:30.55	-60:03:49.50	600	3.0
543.6778981	19:08:30.54	-60:03:49.30	600	2.6
543.6852593	19:08:30.56	-60:03:48.00	600	3.0
543.6902373	19:08:31.18	-60:03:48.80	10	3.0
543.6916250	19:08:31.17	-60:03:49.30	120	3.0
-	-	-	10	3.6
543.6964306	19:08:31.22	-60:03:49.50	600	3.1
543.7038657	19:08:31.15	-60:03:49.60	600	3.8
543.7112454	19:08:31.15	-60:03:50.60	600	3.5
543.7889097	19:08:30.58	-60:04:01.50	10	3.0
543.7902778	19:08:30.71	-60:04:01.50	120	3.4
543.7950880	19:08:30.63	-60:04:01.60	600	3.8
543.8024502	19:08:30.73	-60:04:01.90	600	3.3
543.8098160	19:08:30.72	-60:04:01.40	600	3.3
544.6076713	19:12:56.00	-59:58:56.60	10	4.5
544.6095718	19:12:55.98	-59:58:56.20	120	4.0
-	-	-	10	3.9
544.6143507	19:12:55.95	-59:58:56.20	600	3.3
544.6217569	19:12:55.86	-59:58:55.50	600	3.1
544.6291181	19:12:55.68	-59:58:54.70	600	3.8
544.6810776	19:11:59.39	-59:58:49.70	3	3.9
544.6822546	19:11:59.34	-59:58:50.10	15	3.9
544.6828403	19:11:59.32	-59:58:49.90	15	4.0
544.6834421	19:11:59.36	-59:58:49.80	15	3.8
544.6840231	19:11:59.30	-59:58:49.70	15	3.9
544.6846146	19:11:59.28	-59:58:50.20	15	3.8
544.8073437	19:12:56.27	-59:58:51.20	10	2.8
-	-	-	10	4.0
544.8157002	19:12:56.22	-59:58:51.10	600	3.3
544.8230671	19:12:56.15	-59:58:50.10	600	3.5
544.8304294	19:12:56.26	-59:58:49.60	600	3.2
-	-	-	120	4.0
-	-	-	600	3.4
-	-	-	600	3.2

Table 6: NGC 6752 Observations (Continued)

JD (2449000.0)	RA	DEC	EXP (sec)	FWHM
-	-	-	600	3.2
542.6978634	19:08:31.15	-60:03:54.40	600	3.3
154.6909606	19:08:12.00	-60:04:01.00	600	2.3
155.7678704	19:08:24.00	-60:03:57.00	150	3.3
155.7716898	19:08:24.00	-60:03:57.00	150	3.4
155.7747685	19:08:24.00	-60:03:57.00	150	4.2
155.7778820	19:08:24.00	-60:03:57.00	150	3.8
155.9076968	19:08:24.00	-60:03:58.00	150	3.9
155.9107986	19:08:24.00	-60:03:58.00	150	3.8
155.9139120	19:08:24.00	-60:03:58.00	150	3.5
155.9169908	19:08:24.00	-60:03:58.00	150	4.1
157.7182407	19:11:58.00	-59:59:31.00	120	3.3
157.7238773	19:11:58.00	-59:59:31.00	600	3.5
158.7797685	19:11:59.00	-59:59:16.00	120	2.9
158.7864815	19:11:59.00	-59:59:16.00	600	3.1

**2.2. Reduction.** The first general task of image processing is to remove detector artifacts and calibrate your raw data. This is required to remove any unwanted signal from your images to increase their S/N. There are several contributions to your unwanted noise. Typically when your CCD camera collects photons from your point source, the pixels in the detector not surprisingly collect anything in its field of view. These include background sky and cosmic rays for instance. Additionally, CCD cameras are not made to perfection. This means that some pixels in the CCD tend to be more sensitive to light than others, raising uncertainty in the brightness of your source. Therefore, to obtain worthy light of an object that one studies, image refining becomes essential and a common part of data processing.

To eliminate this surplus of noise, flat field images are the first thing to be taken on the night of observation. For this research, sky and dome flats were used for reduction. Dome flats are produced before the shutters of the telescope open for data collection. With the use of a white screen inside the dome, light gets casted into it, making it recoil and shed a uniform distribution of light onto the CCD camera. The purpose of this is to conspicuously know what pixels are more bias to



sensitivity. The benefit of dome flats is that they can be taken at any time of the day since the shutters are closed. Sky flats in the other hand work in a different matter such that the objective is to illuminate the CCD by mimicking the night sky intensity, in contrast to lamps used for dome flats. Therefore, for this procedure the shutters open for the accumulation of background sky. Subsequently, these flats get normalized and divided by your raw images as mentioned in detail in the following subsection.

Image Reduction and Analysis Facility-IRAF was the software tool used for reduction and analysis in our data. This tends to be a common use in astronomy imaging. First, all flats accounted for were combined with the use of the *imcombine* task that encompasses your flats into a single output file, conveniently named `combinedb.fits` where *b* denotes the particular filter. This step and therefore for the rest of the reduction process was done twice, one for dome flats and the other for sky flats. During this process, one important thing to be aware was making sure the flats combined were created on the same day since data surveying went on for several nights, and every run had their corresponding flat-fields.

A fundamental part of this new file was getting a hold of its average counts per pixel using *imstat*. This task can give valuable statistics on pixels all around the frame. Carrying out this step by finding the mean count then got divided by the `combinedb` file previously made. The result is a new output file commonly referred to as your `masterflatb`, and if done correctly, the file is now normalized to one in terms of pixel count on the entire image. Finalizing into the last step, you obtain another ratio by dividing your `masterflatb` with your raw images making sure they match the same filter. For this task *imarith* was employed which can divide you frames or numbers, or a combination of both besides the many other things it can do. Figure (1) displays a visual process of the frames arising by applying the tasks in IRAF.

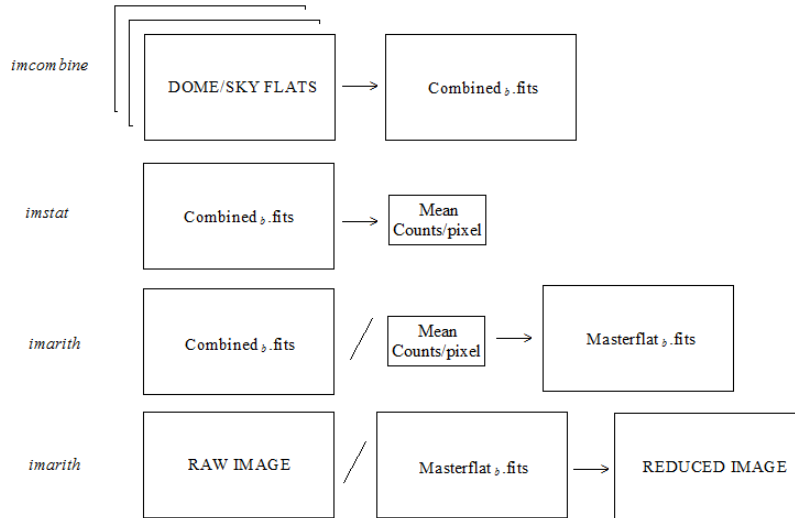


FIGURE 1. **Flat-Field Schematic.** This demonstrates a schematic presentation of the reduction process with the required IRAF tasks to obtain your final processed image. These steps got repeated for the rest of the filter bands, completing data reduction. For our data, this course of action was done once again for the I-band.

### 3. PHOTOMETRY OF STARS

**3.1. Background.** Practically all stars are so far away that they can be considered to be a point source in the sky with no apparent features. However, because of atmospheric aberration, and optical systems having minuscule imperfections, the light entering through the lens of the telescope distributes the light radially making it look blurry. This makes it more of a challenge to obtain the brightness of the star now that the light has spread itself outwardly labeling it as a point spread function (PSF). A PSF is the outcome of a light source that is not defined accurately as a point, but its flux spreads out dispersedly. The goal therefore is to obtain this light of an arbitrary star for photometry use. Photometry is the discipline of measuring the brightness of individual stars in a frame.

**3.2. Selecting PSF Stars.** We carry out the light of the star in an image by encircling it with some aperture under IRAF that is big enough to encompass the light, but small enough to obtain minimum background sky. Once encircled, we

make sure it posses a good PSF by looking at it in a three dimensional plot as illustrated in figure (2).

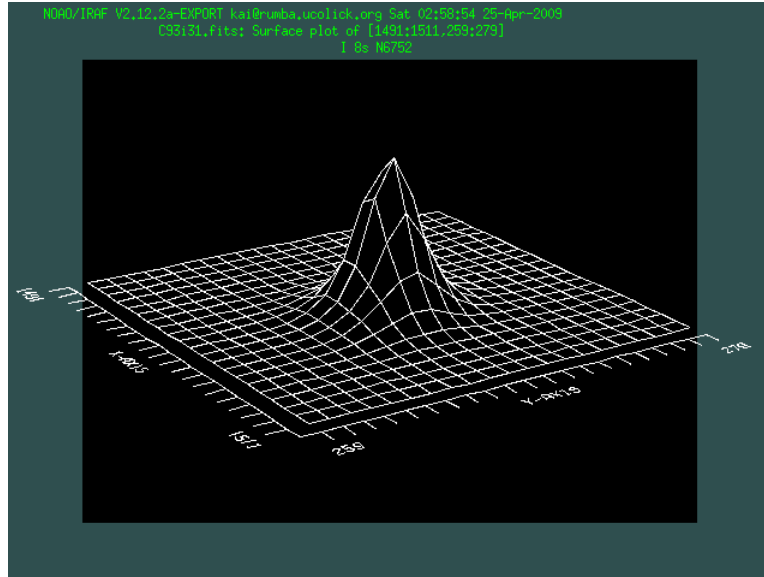


FIGURE 2. **PSF**. A three dimensional display of a good PSF star. 50 or more of such PSFs are essential to achieve convincing magnitudes of stars all around the image.

There is one parameter that needs to be taken into account before the use of a photometry package. We need to know the full width half maximum (FWHM) of a star's intensity which describes how confined or spread out the light is. More precisely, it is the point where the intensity falls down to half its original value. This number varies per star in a single frame but not by much. As for different frames, it can vary more significantly because not all images contain the same time exposure. Roughly speaking, a FWHM can range from 1.5 to 4.5. Because we are looking at an overly populated field, we had to make sure we were very selective with what stars to consider for FWHM. Such stars should contain (a) a good data point fitting on its Gaussian curve (see figure (3)). Some stars are very saturated that they obtain no FWHM. Instead, their pixel values are constant as a function of radius making it appear like a flat line. A star should also be (b) spherically shaped, avoiding elongated stars that probably result from edge effects of the lens.

Finally, (c) it must be an isolated star, otherwise close proximity stars will falsify the brightness distribution. These three parameters have to apply to deem a good FWHM and PSF.

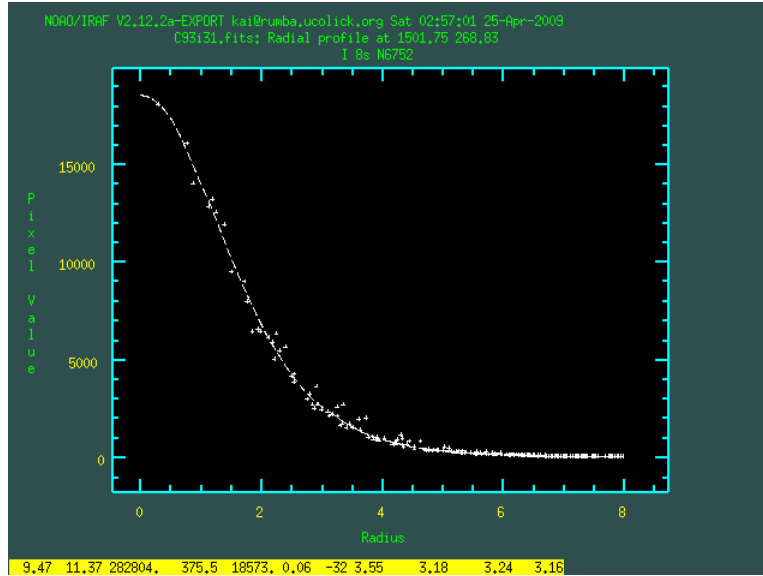


FIGURE 3. **FWHM**. Plotted is the pixel count as a function of the aperture radius. This defines a good FWHM because it contains all data points in the Gaussian. For this particular star the FWHM is equal to 3.16.

A log file consisting of candidate PSF stars with the characteristics just described above were created for every image. Every star was picked manually. The technique was accomplished first by displaying the images with the help of SAOImage DS9 (Joye & Mandel 2002) which is an astronomical imaging application used for viewing frames, afterward IRAF was opened to proceed with the preliminaries. Using *imexam* in IRAF, the task examined the frames with image displays as seen on both figures (2) and (3). After encircling a star with some aperture, clicking “a” gave vital statistics of the selected object. Parameters like pixel coordinates, magnitude, flux, and most importantly FWHM of a star were provided just to mention a few. These stars along with their statistics were saved on a log with file extension *.can* meaning “candidate”. This was manually done for all 199 images, and 50+ stars

were selected per frame. These log files become important to sustain because later on, a script developed to run multiple files simultaneously requires a set of stars to work with under a photometry package.

**3.3. PSF Fitting To Measure Stellar Brightness: Daophot.** Photometry was performed using DAOPHOT II (Stetson 1987) as the stellar photometry package which works wonderful for crowded fields just like in GCs. In order for Daophot to run, three fundamental parameter files have to be created before it can work accordingly. They should be named *daophot.opt*, *photo.opt*, and *allstar.opt* otherwise the program will not recognize them<sup>6</sup>. These files contain parameters like the mean FWHM, saturation limit, radius of aperture, and many other essential values required by the program to search for good stars.<sup>7</sup>

While the preliminary process was obtaining candidate stars with convincing FWHM and PSFs, Daophot automatically takes care of this manual procedure with *Pick*, and creates an output file of all the stars per frame believed were best for photometry. Furthermore, the command *Pick* asks how many stars to consider, and at what magnitudes. Once Daophot does its best job of picking the most exceptional stars, it gives an output extension *.lst* listing the chosen candidate PSFs. Following this, the *PSF* command compiles it providing the final extension file *.psf* with your PSF stars. The photometry package in effect provides numerous output files (*.coo*, *.ap*, *.nei*,... *etc.*) but the majority of them become extraneous for continuation. Extension's *.coo* and *.ap* for example are the preliminary files before obtaining *.lst* and *.psf*, but are inapplicable thereafter and as a result are not discussed.

Although Daophot has the convenience of automatically selecting what it believes are good PSF stars from an image, it then became apparent that the stars considered were chosen very poorly. For reasons that we are still unsure of, the

<sup>6</sup>Trivially its important that these files are maintained within the same working directory or else the photometry package will not run.

<sup>7</sup>For further explanation of these parameters, they are discussed more elaborately by B. Harris & H. Jerjen in <http://msowww.anu.edu.au/jerjen/daophot.html>

package acknowledged all sorts of stars including saturated ones which is what we were trying to avoid in the first place. This is the primary reason why log (*.can*) files were created. Hence, the manual depicting process became the alternative to indemnify for the unacceptable stars acquired by Daophot. Because this step was done manually unfortunately, the continuing output files necessary could not be derived by the program because it did not create its preliminary files. This situation caused for a different direction to obtain them.

Luckily, a script file developed by Dr. Michael Bolte filled in for this discrepancy. Working in conjointment with the photometry package, it ran all the *.can* files simultaneously which was beneficial because Daophot only works with one frame at a time. Moreover, the script conveniently produced *.als* and *s.fits* files administered by the program ALLSTAR that are crucial for proceeding. Allstar is a separate program that works in conjunction with Daophot. What it does is it finally subtracts the star's light leaving only noise as the aftermath of your original image. File *.als* stores these new magnitudes along with other parameters like its x & y coordinates, magnitude error, local sky value, number of iterations, chi, and diagnostic check number. The frame after the light source extraction can be seen on *s.fits*. As part of the procedure, it was important to view every single *s.fits* file making sure the subtraction process was done appropriately. Figure (4) gives a comparison of a star field before and after the subtraction.

**3.4. Matching Stars Measured On Different Frames: Daomatch.** After the course of photometry, DAOMATCH was used to overlap all images that pertain to the same region of the cluster. It produces a *.mch* file that stands for “match”. This is a basic step that can eventually lead one to know how your stars vary over the course of time. Selecting a fiducial frame as your fixed image, every other frame you acquaint it with gets transformed with respect to it. More specifically, it superimposes the stars correspondent on each frame. A fiducial frame has to be an image that outmatches the rest of your data. Relatively, it should be one of the clearest frames, and contain an intermediate time exposure just as importantly. For

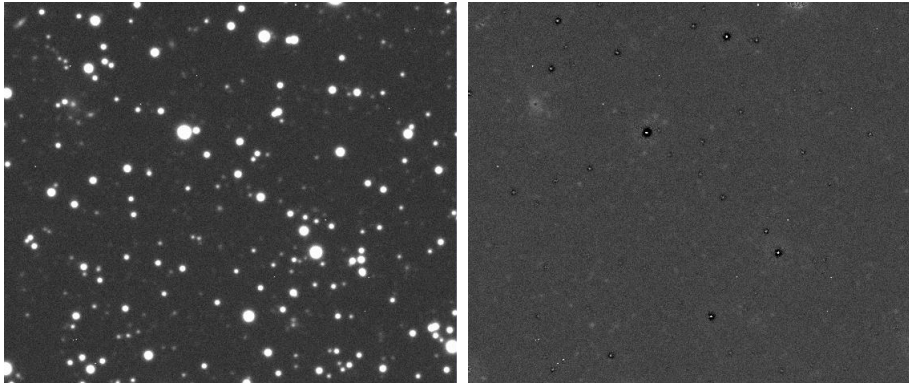


FIGURE 4. **Subtracted Image.** Image on the left demonstrates an unaltered frame as taken on the night of observation. Image on the right is the outcome after analysis was used to fit the brightness profiles of all stars and digitally subtract them from the image. As one can see, all is left is background noise only subtracting star light as expected.

example, if one carries images that range from 1 to 10 seconds, the best frame to consider as your fiducial should be a 5 second exposure. The reason for this is that images with low exposure may not collect enough photons to acquire many stars in your image. On the other hand, images with long exposures will collect sufficient light that more stars will be visible. The only problem with long exposures are that bright stars will become saturated, and will not be useful for time series analysis. In fact, because more faint stars will be present, matching them with frames of short term exposure will likely not appear, becoming unusable for comparison. Therefore, mean exposures are of best choice, making it able to match all time ranges. We attained 120 second exposures as the most ideal for our fiducial frames. In order to do this matching, *.als* are the input files. All data from the same region of the sky should be matched of course. Despite being a simple procedure, various problems were encountered. While Daomatch gives the offset coordinates with respect to the fiducial, some were not correct. Half of them had to be adjusted manually making sure they met the accurate offsets. Lastly, an interesting note to point out here is that by using Daomatch, one can also match frames of different filters. Its meaning will be explained in the upcoming section and its relevance to the research.

### 3.5. Combining Photometry For Stars Measured On Different Frames:

**Daomaster.** After images were matched correspondingly, Daomaster ran *.mch* and gave three important output files. These are *.mag*, *.cor*, and *.raw*. But based on the purpose determines if all are necessary or not. A program design by Dr. Michael Bolte was used in conjunction with Daomaster to combine parameters that are otherwise two files running the program itself (*.mag* and *.raw*). The quality about this is that it lists a table of important values that will become important before and after finding EBs. This table besides containing the magnitudes also have the colors of the stars calculate. With this, a color versus magnitude diagram can be constructed to know more about the cluster stars. This also can be done in Daomaster. It also obtains E/I and chi readings which will be explain in more detail in the following section. The output file produced by Dr. Bolte’s program was named *.icmd* that stands for “instrumental color-magnitude diagram.”

## 4. DISCUSSION

There are steps to identifying EBs. The first is to make a few star selections from a E/I versus Chi diagram and make visual inspections of these stars. Afterward, we extract all zero point-adjusted photometric measurements for each candidate and associate the time with the measurement. Finally, we search with phase dispersion minimization (PDM) for periodic signal. This process helped reduce a great number of stars down to just a few for flux variations. Otherwise searching for light variability in thousands of stars would be an endless process.

**4.1. E/I vs. Chi.** External-to-internal (E/I) is a ratio between the magnitude variance of a star over every frame and the average magnitude error uncertainty for individual points. The variance and mean is given by  $\sigma^2 = \frac{\sum (m_i - \bar{m})^2}{N-1}$  and  $\bar{\sigma} = \frac{\sum \sigma_i}{N}$  respectively. Hence, E/I gives the quotient

$$E/I = \frac{\sum (m_i - \bar{m})^2}{N-1} \left[ \frac{\sum \sigma_i}{N} \right]^{-1}$$



For a possible candidate, E/I has to be a high number. For example, you may have a frame where a binary is distinguished to be two separate stars. On another frame, the seeing that night might have been bad that both stars blended as a single star. This causes variations in the magnitude, and a high E/I value therefore implies a big change from the mean  $\bar{m}$  with small error bars. Figure (5) demonstrates the likelihood of binaries with low  $\chi^2$  values suggesting that these can be potential candidates.

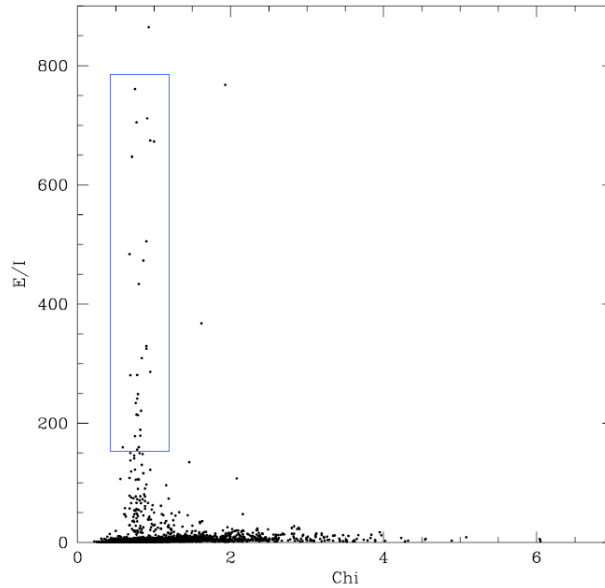


FIGURE 5. **E/I vs. Chi.** Data points enclosed in blue are candidate stars that are possibly binaries. This plot corresponds to data taken in '94 having combined V and I-band filters in Dao-match.

**4.2. Star Inspection.** Using *tvmark* in IRAF helped display the x & y coordinates of the prospecting candidates in the image by encircling them. This lets us know where they are positioned in the image. We made sure they were isolated from companion stars in its vicinity, otherwise magnitude variation could be explained by stars being close to superposition from our line of sight. An example of this is

seen in figure (6); It gives a comparison of a star that is legitimately far from the rest, and another that is overwhelmingly close.

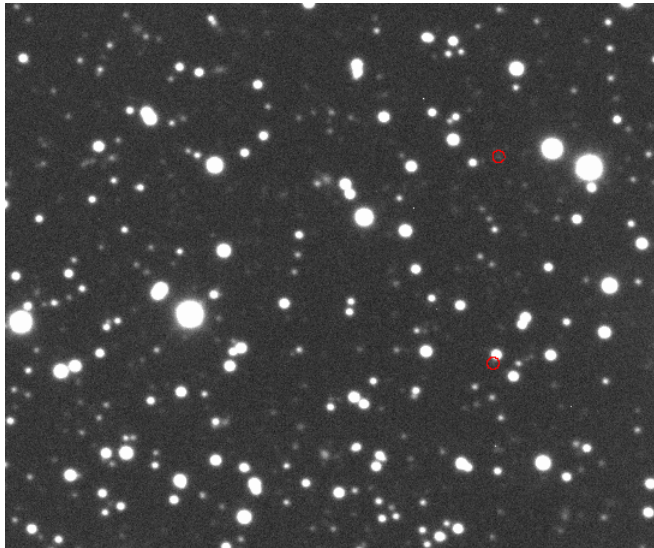


FIGURE 6. **Candidate Stars** The two stars encircled in red demonstrate the high E/I and low chi readings. As a comparison, one of them (top right) shows it to be a fairly distant from the other companions. In contrast the secondary (bottom right) fails to be reliable being next to a highly bright one

**4.3. Periodic Signals.** IRAF becomes very important at this part of the binary search. After choosing stars with low chi and high E/I, and physically looking at their location in the image, individual files consisting of julian days, magnitude, and magnitude error were produced. These files were named after the star number that the *.cor* file accords it. A *.cor* file contains all associated magnitudes of a star that got compared with from a set of images. If these stars hold to be true binaries, their periods will be found by using the phase dispersion minimization (PDM) method (Stellingwerf 1978). This is a task in IRAF conveniently named *PDM*. Essentially, PDM takes all your data points that may seem scattered with no apparent pattern when plotted, and tries to issue it a period that would fit most of your data points. After numerous trials and if it follows a legitimate pattern,

it picks the most suitable period, and as a result a light curve should emerge <sup>8</sup>. Since data was taken in consecutive years, images of '94 in the V-filter are being momentarily examined, followed by the I-band filters. With the anticipation of finding several binaries, the hope is to confirm them with data of a different year and band filter. As a note, the year arrangement is not consequential.

## 5. COLOR-MAGNITUDE DIAGRAM

**5.1. Background.** A color-magnitude diagram (CMD) graphs the magnitude of a star as a function of color. Figure (7) shows the characteristics of a CMD. This serves as an important use in stellar astronomy because it can provide many properties of a star. For example, knowing the color of a star can lead to know its magnitude, temperature, and luminosity ratio with respect to our sun. With careful look at figure (7), the black narrow band is what is called the main-sequence. These are stars that are burning their hydrogen in their cores, and do so for the most part of their lives. The cut off at the top of the main-sequence is called the main-sequence turn off, and these are stars that are at the brink of losing what is left of their hydrogen supply. Stars will settle here for a fraction of their time and ultimately move around in different regions of the graph depending how massive they are.

**5.2. Candidates on the CMD.** A deep CMD of NGC 6752 in the long and short exposure were created and overlapped. Based on evolutionary model fittings for turn off points, NGC 6752 estimates an age of  $13.8 \pm 1.1$  Gyrs (Gratton et al. 2003) after observations made by the Wilkinson Microwave Anisotropy Probe (WMAP). Stars boxed in red on figure (8) are the candidates showing where they are located in the CMD. Based on their location, it becomes apparent that the majority of them seem to settle on the narrow band, making them main-sequence stars. Despite there being several binary potentials, only a small number of these

---

<sup>8</sup>Further description of PDM can be looked at in <http://hea-www.harvard.edu/swolk/thesis/period/node2.html>

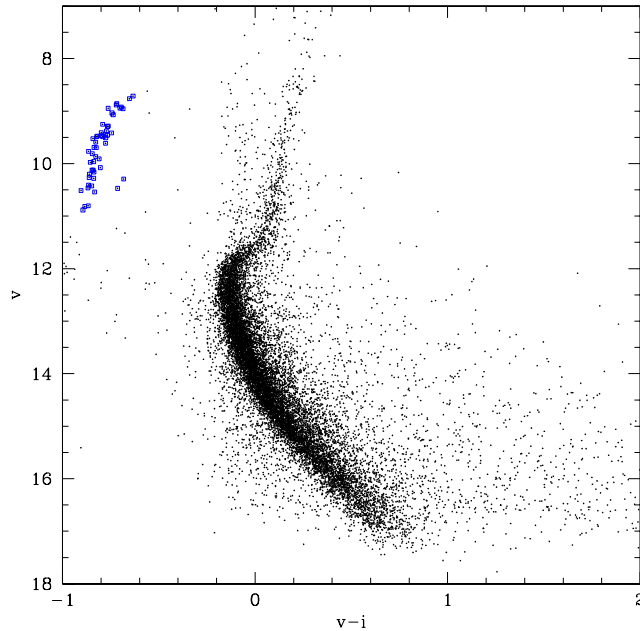


FIGURE 7. **Short CMD of NGC 6752** The vertical axis is the magnitude in the visible (V) spectrum and the horizontal axis is color (V-I). Color is determined by the difference of magnitude as seen in two filters i.e. V-I. The CMD was constructed from a short exposure. Stars boxed in blue are the blue horizontal branch that are the hottest of them all burning helium in their cores.

will truly be EBs or of any other classification of binaries. The ultimate test will be using *PDM* in IRAF that will establish a period if something is there.

**5.3. Artificial Star.** To make sure *PDM* was a reliable program, we added an artificial star obtained by StarLight Pro 2.1.22<sup>9</sup>. We defined it with a specific period and amplitude, and the hope was that *PDM* would return these parameters back accurately. The artificial star contained a total of 144 data points. A presentation of the result is shown in figure (9). Because our real data contains one-third of the data points, we extracted the majority of them from the artificial star to see if it could reliably provide the given parameters still. We subtracted 128 number points, and fortunately the program responded very well. Figure (9) therefore illustrates

<sup>9</sup>Direct link to this program is found in <http://www.midnightkite.com/binstar.html>

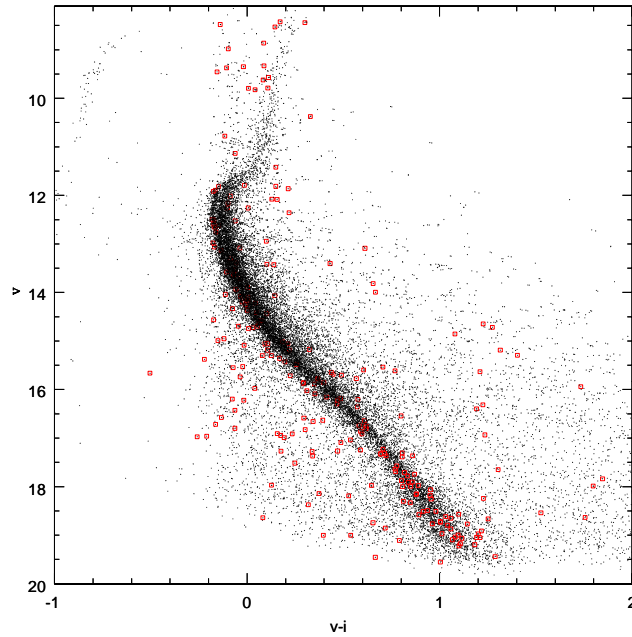


FIGURE 8. **Deep CMD of NGC 6752.** This CMD was combined from a long and short exposure. Boxed stars are all the possible binaries that may be present on the East side of the cluster.

number point comparisons for this artificial star. One with all its data points, and the other with 16 after the extraction.

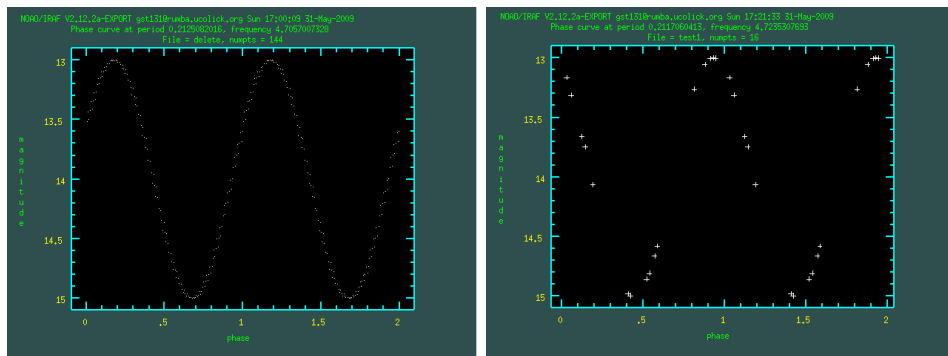


FIGURE 9. **Artificial Star** These two diagrams are plotted in magnitude versus phase. The left graph contains all the original (144) data points. Graph on the right contains only 16 but as one can easily see, both display a very well defined sinusoidal pattern.

5.4. **Detections.** After promising results from the artificial star, we then took up real data to begin detecting for any variabilities. Two light curves turned out to be very promising showing reasonable light variations. Star 5996 is a main-sequence star that carries a period of  $P = 0.6109$  days which is consistent with previous period detections given by Thompson & Kaluzny et al. 1999. It consists of 38 data points and it is still undetermined in terms of what class of binary we are looking at. Figure (10) graphs a light curve in magnitude as a function of phase, illustrating the sinusoidal pattern. The error bars were also included to display the uncertainty in the magnitude, and even then does it look feasible that this star is more than just constant over time. The star contains a magnitude of  $M_0 = 17.325$  on the CMD in figure (8), although this number specifically carries no meaning because the binary varies in flux.

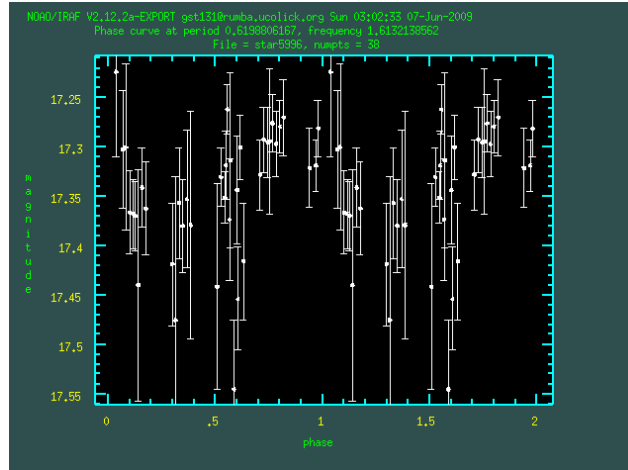


FIGURE 10. **Star 5996 Light Curve.** This is a light curve of star 5996 displaying a pattern that looks to be continuous. Its frequency is  $\nu = 1.61321$  with an amplitude of  $M_0 = 0.32120$ . Despite being a recent detection, it still remains uncertain of its binary class.

Star 5000730 is another light curve that seems to be sequential. The period is one-third that of star 5996 with a value of  $P = 0.24209$  days. Because it is a small period, this implies that perhaps it is close to its companion star in their orbit. The amplitude is  $M_0 = 1.48840$  which is very significant based on its dimness.

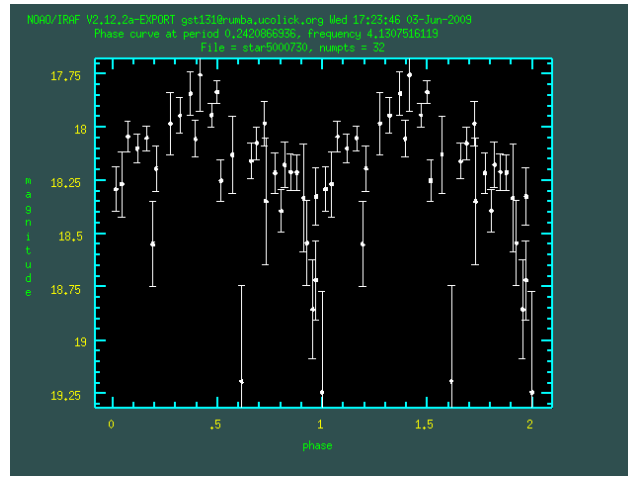


FIGURE 11. **Star 5000730 Light Curve.** A light curve of star 5000730. Its frequency is  $\nu = 4.13075$  with an amplitude of  $M_0 = 1.48840$ . This one in comparison to star 5996 has less uncertainty in the magnitude error bars, and it is also fainter in magnitude.

TABLE 7. Light Curve Parameters

ID	Period (Days)	$M_0$	RA	DEC	Frequency ( $\nu$ )	$V - I$
5996	0.61988	0.32120	19:13:03.39	-59:59:57.1	1.61321	0.694
5000730	0.24209	1.48840	19:12:02.50	-59:51:49.6	4.13075	0.878

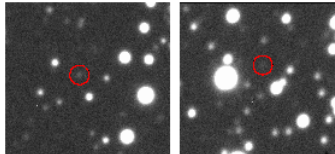


FIGURE 12. **Star 5996 and 5000730 Location.** Encircled in red is star 5996 and 5000730. They are both located on the East side of the cluster, and their RA and DEC can be found under Table(1).

The light curve of star 5000730 can be seen on figure (11). Both stars are very dim with magnitudes ranging in the +17 and +18. They were found in long exposure images. As a comparison of these two, our sun has a magnitude of -26.0, and the faintest stars one can see in the darkest and clearest nights are of order +5.0 magnitude. Based on detections previously provided by other groups, these

stars are considered to be newly discovered binaries. Table (1) gives a summary of the key parameters.

## 6. CONCLUSION

CCD photometry was performed in NGC 6752 with filters in the I and V-band. Despite the project being under current search for EBs, star 5996 and 5000730 have been found to be potential variables based on their light curves. Results demonstrate that their parameters are very reasonable in comparison to other detections made in this cluster. As the search continues, it is expected that various other stars will be predetermined based on locality of where we are searching. In a publication coming soon, will we have more robust detections that will give further convincing evidence that clusters are prevented from core collapse by the abundances of binaries.



## REFERENCES

- [1] Jones, M. H., & Lambourne, R. J. A. (2003). An introduction to Galaxies and Cosmology. Cambridge: Press Syndicate of the University of Cambridge.
- [2] Harris, W.E. 1996, AJ, 112, 1487
- [3] R. G. Gratton, 2003, A&AS, 408, 529
- [4] Thompson, I. B, Kaluzny, J., Pych, W., & Krzeminski W. 1999, AJ, 118, 462
- [5] Kaluzny, J., & Thompson, I. B.
- [6] Joye, W.A, & Mandel E. 2003, ASPC..295..489J
- [7] Stetson, P. B. 1987, PASP, 99, 191
- [8] Stellingwerf, R. F. 1978, AJ, 224, 953

UCO/LICK OBSERVATORY, UNIVERSITY OF CALIFORNIA, SANTA CRUZ CA 95064

*E-mail address:* [cahernan@ucsc.edu](mailto:cahernan@ucsc.edu)